Chemical Engineering Journal 157 (2010) 52–59

Contents lists available at ScienceDirect

Chemical Engineering Journal

journal homepage: www.elsevier.com/locate/cej

Combined effects of thermophoresis and electrophoresis on particle deposition onto a vertical flat plate from mixed convection flow through a porous medium

R. Tsai [a], J.S. Huang [b,*]

[a] Department of Mechanical Engineering, Chung Yuan Christian University, Chung Li, 32023, Taiwan
[b] Department of Architecture, National Taiwan University of Science and Technology, Taipei 106, Taiwan

ARTICLE INFO

Article history:
Received 24 July 2009
Received in revised form 18 October 2009
Accepted 19 October 2009

Keywords:
Particle deposition
Thermophoresis
Electrophoresis
Filtration processes
Porous medium
Indoor air quality

ABSTRACT

Suspended dust particles are usually correlated to indoor air quality, filtration processes, and environmental problems. Dealing with air mixed with suspended particles is a matter of great urgency. This paper presents a theoretical study on aerosol particles responding to thermophoresis, electrophoresis and the particle deposition rate onto a vertical flat wall with wall heat flux in a porous medium. The non-Darcian model is employed to analyze this process. The flow is modeled as a two-dimensional, incompressible, steady-state laminar mixed convection flow. The particle transport mechanisms are promoted by convection, Brownian diffusion, thermophoresis and electrophoresis. Similarity analysis is used to transform the governing equations for continuity, momentum, energy and concentration into a system of partial differential equations. Using numerical techniques, the particle concentration profiles and deposition velocities are obtained to improve the particle filtration technology and remove contaminants from the air.

1. Introduction

Aerosol particles are a kind of airborne pollution. The deposition mechanism due to thermophoresis and electrophoresis is important for indoor air quality engineering applications. The technological problems correlating to particle deposition onto wafers in the microelectronics industry play a critical role in the product quality yield rate. Particles which impact the blade surface of gas turbines are produced by condensing vapor–gas mixtures. Other applications are filtration in gas-cleaning, nuclear reactor safety, electrostatic precipitators, clean room and human health topics. Controlling the particle transport path is a significant issue. The factors that affect particle transport include convection, Brownian diffusion, turbulence, sedimentation, inertial effect, thermophoresis, electrophoresis and surface geometry. Generally speaking, thermophoresis can be effective in moving submicron particles within a range of 0.01–1.0 μm. Convection, Brownian diffusion and electrophoresis are important for particles smaller than 0.1 μm. The inertial effect and sedimentation are significant for particle diameters larger than 1.0 μm. We chose particle Schmidt numbers (Sc_p) corresponding to particle sizes of 0.01–1.0 μm and discuss the particle transport phenomenon under combined effects. Hence, convection, Brownian diffusion, thermophoresis and electrophoresis are the main effects for particle diffusion in this case [1].

Goldsmith and May [2] pioneered a study on the thermophoretic transport involved in a simple one-dimensional flow for thermophoretic velocity measurements. After that, Goren [3] developed the thermophoretic deposition of particles in a laminar compressible boundary layer flow past a flat plate. Talbot et al. [4] numerically solved the momentum and energy fields for a laminar boundary layer adjacent to a hot wall surface. Recently, Chamkha and Pop [5] showed the thermophoretic force effect in the free convection boundary layer from a vertical flat plate embedded in a porous medium. Seddeek [6] studied the heat and mass transfer for mixed convection flow about an isothermal vertical flat plate embedded in a fluid-saturated porous medium with the viscous dissipation and thermophoresis in both aiding and opposing flows.

Works on the coupled effects of thermophoresis and electrophoresis were presented. Peterson et al. [7] used the boundary layer approximation and perturbation methods to solve the transport equation and determine the particle deposition rate. Peters and Cooper [8] followed the method by Friedlander et al. [9] to analyze the effects of electrostatic force on thermophoretic suppression of particle diffusion deposition onto hot surfaces. Opiolka et al. [10] carried out experiments and used the simply stagnant film model to examine the deposition rates. Tsai et al. [11] proposed a theoretical study of aerosol particles responding to thermophoresis, electrophoresis and the particle deposition rate onto an axisymmetric wafer. Comparing the calculated deposition velocity results

* Corresponding author. Tel.: +886 3 2854020; fax: +886 2 27376721.
E-mail addresses: lilysonq@yahoo.com.tw, g1213991@ms36.hinet.net (J.S. Huang).

1385-8947/$ – see front matter © 2009 Elsevier B.V. All rights reserved.
doi:10.1016/j.cej.2009.10.046

Nomenclature

a	free stream strength [s^{-1}]
A	positive constant
B	particle mobility [$m^2\ V^{-1}\ s^{-1}$]
C	particle concentration
C_c	Stokes-Cunningham correction factor
C_i	Forchheimer inertia coefficient [m^{-1}]
C_s, C_t, C_m	constants in Eq. (7)
d	mean particle or pore diameter of the porous medium [mm]
d_p	particle diameter [μm]
D	mass diffusivity [$m^2\ s^{-1}$]
e	electron charge [C]
E	electric field strength [$V\ m^{-1}$]
f	dimensionless flow stream function
Gr	Grashof number
g	Gravity [$m\ s^{-2}$]
J_w	wall particle flux [$kg\ m^{-2}\ s^{-1}$]
K	Darcy permeability [m^2]
Kn	Knudsen number
k	thermal conductivity [$W\ m^{-1}\ K^{-1}$]
Nt	thermophoretic parameter
n	exponent of heat flux
n_e	elementary charge number
Pr	Prandtl number
q	total electron charge on the particle [C]
q_w	wall heat flux [$W\ m^{-2}$]
Re	Reynolds number
Ri	Richardson number
Sc_p	particle Schmidt number
T	temperature [K]
T^*	characteristic wall temperature [K]
u, v	streamwise and normal velocity components, respectively [$m\ s^{-1}$]
V_d	particle deposition velocity [$m\ s^{-1}$]
V_E	electrophoretic velocity [$m\ s^{-1}$]
V_T	thermophoretic velocity [$m\ s^{-1}$]
x, y	streamwise and normal coordinates, respectively

Greek symbols

α	thermal diffusivity [$m^2\ s^{-1}$]
β_T	volumetric coefficient of thermal expansion [K^{-1}]
γ	inertia parameter
δ_T	thermal boundary layer thickness
ε	porosity
η, ξ	similarity variables
θ	dimensionless temperature
κ	thermophoretic coefficient
λ_g, λ_p	thermal conductivities of air and particle, respectively [$W\ m^{-1}\ K^{-1}$]
μ	air dynamic viscosity [$kg\ m^{-1}\ s^{-1}$]
ν	air kinematic viscosity [$m^2\ s^{-1}$]
ρ	air density [$kg\ m^{-3}$]
ϕ	dimensionless concentration
Ψ	stream function

Subscripts

w, ∞	conditions at the wall and ambient, respectively

with the experimental solutions from previous works showed very good agreement. Later, the wall suction effect and thermophoresis for the particle deposition mechanism on a vertical flat plate were obtained [12].

Darcy's law proved that the pressure drop produced by frictional drag is in proportion to the low speed velocity flow when a fluid flows through a porous medium. When high flow velocity occurs or the Reynolds number exceeds 1 to 10 based on the mean pore or particle diameter of the porous media, Darcy's law is no longer suitable. Non-Darcian effects including the inertia and boundary effects should be also considered. Forchheimer [13] proposed the inertia effect of non-Darcy consideration in making up for the pressure drop when a fluid flows through a porous medium. Moreover, Vafai and Tien [14] discussed a combination of the solid boundary and inertia effects on a porous medium and adopted the local volume averaging technique to derive the governing equations. Plumb and Huenefeld [15], and Vasantha et al. [16] reported on non-Darcy natural convection for different geometries in saturated porous media by employing Ergun's model [17].

Mixed convection is the term describing the fluid flow driven by a combination of forced and natural convection. The flow, thermal and diffusion phenomena may be affected due to the relative directions of buoyancy-induced and forced convection motions. Aiding flow means that the forced and natural convection air currents are in the same direction, whereas opposing flow means that they move in opposite directions. The thermal buoyancy force plays a significant role in forced convection, when the flow velocity is slow and the temperature difference between the surface and free stream is relatively large. Under these conditions, a mixed convection model can predict the flow, heat and mass transfer characteristics accurately. Sparrow et al. [18] carried out an analysis of the boundary layer equations and similarity solutions for combined forced and free convection flows. The result of their study was that the flow can be classified using the parameter Gr_x/Re_x^2. Lloyd and Sparrow [19] used the similarity solutions to discuss the mixed convection under small effect of Gr_x/Re_x^2. Oosthuizen and Hart [20] solved the numerical solution for the constant wall temperature and heat flux problem. To study the combined effects, Ranganathan and Viskanta [21] proposed a mixed convection flow over a horizontal flat plate embedded in a non-Darcy medium with suction and injection effects. The mixed convection flow along a vertical adiabatic surface embedded in a non-Darcian porous medium was numerically analyzed by Jang and Shiang [22]. Recently, mixed convection over a flat plate embedded in a non-Darcian porous medium with suction effect was studied by Elbashbeshy and co-workers [23–25]. The thermophoretic effect was examined on the mixed convection flow over the flat plate to calculate the deposition velocity by Chang et al. [26]. Seddeek [6] studied the influence of viscous dissipation and thermophoresis on Darcy–Forchheimer mixed convection in a fluid-saturated porous medium. Selim et al. [27] discussed the surface mass transfer effect on a mixed convection flow past a hot permeable surface with thermophoresis.

In this work, the particle transport mechanisms over a vertical porous medium with wall heat flux using the coupled effects of Brownian diffusion, mixed convection, non-Darcy, thermophoresis and electrophoresis are examined. A detailed analysis of the influence caused by thermophoresis and electrophoresis due to the temperature gradient and electrostatic force are presented in this study. Still, relatively few published papers have probed into the particle deposition rate under combined effects through a porous medium. In engineering practice, more than one mechanism can act simultaneously and their interactions must be considered for accurate deposition rate prediction. Owing to the extensive applications in industrial and daily life problems, numerical studies have been performed for the convection problems.

2. Mathematical formulation

We consider a two-dimensional, steady, and incompressible laminar flow along a vertical flat wall with heat flux q_w. The

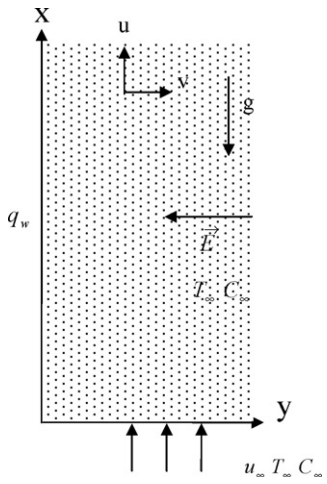

Fig. 1. Schematic of air-particle flow along a flat wall through a porous medium physical model and coordinate system.

ambient temperature and concentration are T_∞ and C_∞. The x-coordinate is measured along the plate from its leading edge and the y-coordinate normal to it. Fig. 1 shows the physical mixed convection flow system over a vertical flat plate through a porous medium. The concentration equation including the thermophoresis and electrophoresis terms are discussed. According to the convection, Brownian diffusion, non-Darcian effects, thermophoretic and electrophoretic transport, the assumption can be stated as follows:

1. The boundary layer approximations are applicable for the flow.
2. The convective fluid and porous structure are everywhere in local thermodynamic equilibrium.
3. Variable porosity and thermal dispersion effects are neglected.
4. The Boussinesq approximation is employed $\rho = \rho_\infty[1 - \beta_T(T - T_\infty)]$ for the flow.
5. The thermophysical properties of the aerosol particles and air are maintained constant.
6. Dilute particle concentrations and negligible particle inertial effects due to low air flow rates and particle concentration at the wall is zero.
7. The electric field strength is uniform in the system.

To discuss the particle transport mechanisms under thermophoresis and electrophoresis, the transformed form of the conservation equations for fluid flow through an isotropic and homogeneous saturated porous medium could be written as follows:

Continuity equation

$$\frac{\partial u}{\partial x} + \frac{\partial v}{\partial y} = 0 \tag{1}$$

Momentum equation

$$\frac{\rho}{\varepsilon^2}\left(u\frac{\partial u}{\partial x} + v\frac{\partial u}{\partial y}\right) = \rho_\infty g\beta_T(T - T_\infty) + \frac{\mu}{\varepsilon}\frac{\partial^2 u}{\partial y^2} - \frac{\mu}{K}(u - u_\infty) - \rho C_i(u^2 - u_\infty^2) \tag{2}$$

Energy equation

$$u\frac{\partial T}{\partial x} + v\frac{\partial T}{\partial y} = \alpha\frac{\partial^2 T}{\partial y^2} \tag{3}$$

Concentration equation

$$u\frac{\partial C}{\partial x} + v\frac{\partial C}{\partial y} + \frac{\partial}{\partial y}[C(V_T + V_E)] = D\frac{\partial^2 C}{\partial y^2} \tag{4}$$

The boundary conditions for Eqs. (1)–(4) are

$$\begin{aligned} &x = 0,\ y > 0,\ T = T_\infty,\ C = C_\infty,\ u = u_\infty \\ &x > 0,\ y = 0,\ q_w = Ax^n,\ C = 0,\ u = 0,\ v = 0 \\ &y \to \infty,\ T = T_\infty,\ C = C_\infty,\ u = u_\infty \end{aligned} \tag{5}$$

where u, v are velocity components parallel and perpendicular to the plate. $u_\infty = ax$ is the free stream velocity, a is a constant which stands for the characteristic free stream strength and the value of $10\,s^{-1}$ is selected in this study. ρ is air density, and g is acceleration due to gravity. ε, K are the porosity and permeability of the porous medium, and β_T is volumetric coefficient of thermal expansion of the fluid. T is temperature, C is particle concentration, ν is kinematic viscosity and C_i is transport property related to the inertia effect. α, D are the thermal and mass diffusivity, respectively. A is a constant and n is exponent of heat flux. The suffixes w and ∞ denote the conditions at the wall and ambient. In the Eq. (2), it is worthy to interpret that $(\mu/K)(u - u_\infty)$ is the term from Darcy's law. $C_i(u^2 - u_\infty^2)$ is the inertia effect suggested by Forchheimer [13]. When the flow rate is high, an additional velocity-squared term should be counted in the momentum equation. $(\mu/\varepsilon)(\partial^2 u/\partial y^2)$ is the boundary viscous effect considering the porosity. The boundary effect becomes significant as the heat transfer occurs near the porous wall region. The Brinkman's extension [28] incorporated a viscous shear stress term into the momentum equation, together with no-slip condition, is used to count for the importance of the solid boundary effect. In order to study the transport mechanisms through a non-Darcian porous medium, the original Darcy model is improved to include the boundary viscous and inertia effects. Moreover, in Eq. (4), the thermophoretic velocity V_T recommended by Talbot et al. [4] is

$$V_T = -\kappa\nu\frac{\nabla T}{T} = -\kappa\nu\frac{1}{T}\frac{\partial T}{\partial y} \tag{6}$$

The value of $\kappa\nu$ represents the thermophoretic diffusivity and κ is the thermophoretic coefficient defined using

$$\kappa = \frac{2C_s(\lambda_g/\lambda_p + C_tKn)C_c}{(1 + 3C_mKn)(1 + 2\lambda_g/\lambda_p + 2C_tKn)} \tag{7}$$

Here, λ_g and λ_p are the thermal conductivities of the air and diffused particles, respectively. C_s, C_t and C_m are determined by experimental data, $C_s = 1.147$, $C_t = 2.20$ and $C_m = 1.146$; $C_c = 1 + Kn(C_1 + C_2\exp(-C_3/Kn))$ is the Stokes-Cunningham correction factor and Kn is the Knudsen number, $C_1 = 1.2$, $C_2 = 0.41$ and $C_3 = 0.88$ [29]. The value of κ can be taken as ranging from 0.2 to 1.2, a representative value for particle smaller than 1 μm is 0.5.

V_E is the electrophoretic velocity as if we put an electron charged particle into a uniform electric field and the particle would be driven to the plate by tracing the direction of the electric field. The spherical particle velocity starts from zero initially and gradually increases to reach the force balance of Coulomb and Stokes drag, which is so called the terminal electrostatic velocity and electrical drift velocity [11,30]

$$V_E = \frac{qC_c\vec{E}}{3\pi d_p\mu} = B\vec{E} \tag{8}$$

$$q = n_e e \tag{9}$$

$\mu = 1.6 \times 10^{-5}\,kg\,m^{-1}\,s^{-1}$ is the air viscosity and B is the particle mobility, respectively. E, e and n_e are electric field strength, electron charge, and elementary charge number. Here, $e = 1.6 \times 10^{-19}$ coulomb stands for unit electron charge and q means the total electron charge on the particle. We choose particle sizes in a range of $d_p = 0.01$–1.0 μm which coincide with correction factor of $C_c = 22.45$–1.166. The uniform electric field strength E equals to 0–10,000 V/m and the electron charge $n_e = 1$–100 are selected. Substituting these parameters to the Eq. (8) and the electrophoretic velocity could be calculated.

The solid–fluid combination porous medium is used in this study. The values of permeability K and inertia coefficient C_i are calculated by employing the Ergun's model [17,24]

$$K = \frac{d^2\varepsilon^3}{150(1-\varepsilon)^2} \tag{10}$$

$$C_i = \frac{1.75(1-\varepsilon)}{\varepsilon^3 d} \tag{11}$$

In the mixed convection model the buoyancy driving force is induced by the thermal expansion term under the Boussinesq approximation. Using the scale analysis, the governing equations could be transformed by introducing a dimensionless stream function, $f(\xi,\eta)$ dimensionless temperature, $\theta(\xi,\eta)$ and dimensionless concentration, $\phi(\xi,\eta)$ accompanied with the following similarity variables

$$\eta(x,y) = \frac{y}{x}Re_x^{1/2},\ \ \xi(x) = \frac{x^2}{K}Re_x^{-1},\ f(\xi,\eta) = \frac{\psi(x,y)}{\nu Re_x^{1/2}},$$
$$\theta(\xi,\eta) = \frac{T-T_\infty}{T^*}Re_x^{1/2}, \tag{12}$$
$$\phi(\xi,\eta) = \frac{C}{C_\infty},\ Nt = \frac{T_\infty}{T^*}Re_x^{1/2},\ T^* = \frac{xq_w}{k}$$

where $\Psi(x,y)$ is the stream function that satisfied Eq. (1) with $u = \partial\Psi/\partial y$ and $v = -\partial\psi/\partial x$.

Substitute Eq. (12) into Eqs. (2)–(4), we could obtain the following system.

$$\frac{1}{\varepsilon}f''' + \frac{1}{2\varepsilon^2}ff'' + Ri\xi^{1/2}\theta - \xi(f'-1) - \gamma\xi(f'^2-1)$$
$$= \frac{\xi}{\varepsilon^2}\left(f'\frac{\partial f'}{\partial\xi} - f''\frac{\partial f}{\partial\xi}\right) \tag{13}$$

$$\frac{1}{Pr}\theta'' + \frac{1}{2}[f\theta' - (1+2n)f'\theta] = \xi\left(f'\frac{\partial\theta}{\partial\xi} - \theta'\frac{\partial f}{\partial\xi}\right) \tag{14}$$

$$\frac{1}{Sc_p}\phi'' + \left[\frac{1}{2}f + \kappa\frac{1}{Nt+\theta}\theta' - V_E(va)^{-1/2}\right]\phi'$$
$$+ \left[\kappa\frac{1}{Nt+\theta}\theta'' - \kappa\left(\frac{1}{Nt+\theta}\right)^2(\theta')^2\right]\phi = \xi\left(f'\frac{\partial\phi}{\partial\xi} - \phi'\frac{\partial f}{\partial\xi}\right) \tag{15}$$

where the primes denote partial differentiation with respect to η.

T^* is the characteristic wall temperature and k is thermal conductivity. $Pr = \nu/\alpha$ is the Prandtl number in which the value chosen for the air equals to 0.7 in this case and $Sc_p = \nu/D$ is the particle Schmidt number. $Ri = Gr_x/Re_x^2$ is the Richardson number with the physical meaning standing for the mixed convection intensity, ($Gr_x = K^{1/2}g\beta_T T^* x^2/\nu^2$ is the modified Grashof number and $Re = u_\infty x/\nu$ is the Reynolds number) which represents the intensity of natural convection relative to forced convection. For $Ri > 0$, stands for the buoyancy force and free stream in the same direction (aiding mixed convection). $\gamma = C_i K u_\infty/\nu$ represents the dimensionless inertia parameter expressing the importance of the inertia effect and Nt is the thermophoretic parameter which corresponds to the driving force act on the diffusing particles due to temperature gradient.

The transformed boundary conditions for Eq. (5)

$$\eta = 0, f(\xi,0) = 0,\ f'(\xi,0) = 0,\ \theta'(\xi,0) = -1,\ \phi(\xi,0) = 0$$
$$\eta \to \infty, f'(\xi,\infty) = 1,\ \theta(\xi,\infty) = 0,\ \phi(\xi,\infty) = 1 \tag{16}$$

Of great interest to the particle deposition velocity under mixed convection flow, we could perform further study to calculate the velocities for various particle sizes.

Table 1
Wall shear stress $f''(1,0)$ and temperature $\theta(1,0)$ at $Pr = 0.7$, $Ri = 1.0$, $\gamma = 2.01$, $\varepsilon = 0.45$.

n	$f''(1,0)$ Elbashbeshy and Bazid [24]	Present study	$\theta(1,0)$ Present study
0.0	1.69	1.70	1.73
0.5	1.62	1.62	1.45
1.0	1.58	1.57	1.29
1.5	1.55	1.54	1.18
2.0	1.53	1.52	1.10

Particle deposition flux to the wall surface can be determined using the definition

$$J_w = D\left.\frac{\partial C}{\partial y}\right|_{y=0} = D\phi'(\xi,0)\frac{1}{x}Re_x{}^{1/2}C_\infty \tag{17}$$

The deposition velocity is customarily defined as the particle flux divided by the free stream concentration

$$V_d = \frac{J_w}{C_\infty} = D\phi'(\xi,0)\frac{1}{x}Re_x{}^{1/2} = \frac{1}{Sc_p}\phi'(\xi,0)\sqrt{av}$$
$$= \frac{1}{Sc_p}\phi'(\xi,0)u_\infty Re_x{}^{-1/2} \tag{18}$$

or written in a dimensionless form

$$\frac{V_d}{u_\infty}Re_x{}^{1/2} = \frac{1}{Sc_p}\phi'(\xi,0) \tag{19}$$

where $\sqrt{av}$ denotes a characteristic velocity of the free stream, $(V_d/u_\infty)Re_x{}^{1/2}$ is defined as a ratio between the fluid flow time, x/u_∞, and the particle deposition time in the thermal boundary layer, δ_T/V_d ($Re_x^{1/2}$ is of the order of x/δ_T for laminar air flow). Commonly, V_d/u_∞ is also called the particle Stanton number in the classical text books for mass transfer with the number denoting $St_p = J_w/u_\infty C_\infty$ [1].

3. Results and discussions

Because the Eq. set (13) and (14) is still a form of partial differential equations due to the nonsimilar terms on the right-hand side, we adopted the box method associated with the block-elimination scheme (suggested in books by Isaacson and Keller [31], and Cebeci and Bradshaw [32]) to solve the velocity and temperature fields. The grid mesh selected is $\Delta\eta = 0.01$. The results obtained for the wall shear stress $f''(1,0)$ and temperature $\theta(1.0)$ are shown in Table 1. The table shows very good agreement in the wall shear stress between our calculations and the data presented by Elbashbeshy and Bazid [24]. Usually, the particle Schmidt number for aerosols is very large ($\geq 10^3$) and the resulting concentration boundary layer is much thinner than the hydrodynamic and thermal boundary layers. Because of $\partial/\partial x \ll \partial/\partial y$ in the concentration boundary layer, the effect due to the terms on the right-hand side of Eq. (15) is insignificant using the order of magnitude analysis. The concentration solutions are obtained using the fourth-order Runge–Kutta integration with a shooting scheme and five-decimal accuracy as the convergence criterion.

Brownian diffusion, thermophoresis and electrophoresis play a vital role for small particles $d_p \leq 0.1\,\mu m$. For large particles $d_p \geq 1.0\,\mu m$, the inertial deposition and sedimentation become important. Particle sizes which are used to examine the thermophoretic and electrophoretic velocity are selected in a range of 0.01–1.0 μm corresponding to the Schmidt number values from 2.83E+02 to 5.46E+05. In this case, the thermophoretic parameter is defined as a function of the free stream temperature and the characteristic wall temperature. The thermophoretic parameter is expressed as a form of $Nt = (T_\infty/T^*)Re_x^{1/2}$. For maintained ambient

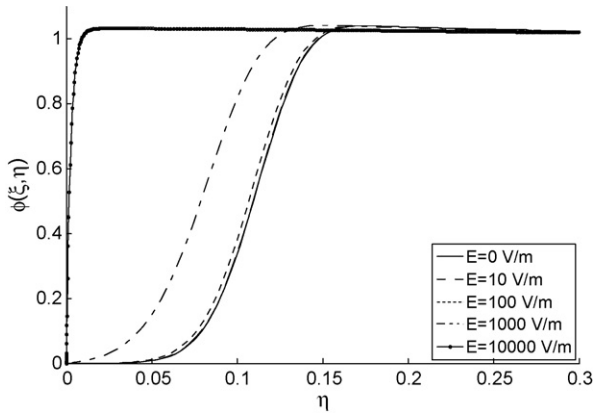

Fig. 2. Particle concentration profiles for different electric field strengths at $\xi = 1.0$, $n = 1.0$, $d_p = 0.1$ μm, $Ri = 1.0$, $\gamma = 2.01$, $\varepsilon = 0.45$, $a = 10$, $\kappa = 0.5$, $n_e = 1$, Nt = 100.

temperature, the larger Nt coincides with a smaller characteristic wall temperature at a constant free stream velocity. Hence, the thermophoretic effect decreases because of the smaller characteristic wall temperature and temperature gradient. After the velocity and temperature fields are solved, the particle concentration profiles can be obtained from the particle transport equation including the effects of diffusion, mixed convection, thermophoresis and electrophoresis. The interactive effects for the particle concentration transport and deposition velocity are depicted from the concentration profiles.

Figs. 2 and 3 illustrate the dimensionless particle concentration profiles at different electric field strengths for Nt = 100 and 1000. From the profiles, we can determine that the gradually enhancing electric field coincides with the thinner boundary layer thickness and this phenomenon occurs because of the suction effect. Moreover, the $E = 0$ V/m equals the zero suction effect caused by the electrostatic force. As Nt = 100 in Fig. 2, the particles are driven away from the surface by thermophoretic force leading to a zone free of particles. Fig. 3 reveals as Nt = 1000 corresponds to the weaker thermophoretic effect than Nt = 100. The concentration profiles all rise steeply at $\eta \to 0$, indicating a large particle flux and the slope of the profiles increase with increasing E for a larger suction force.

Figs. 4 and 5 show the particle concentration profiles for different thermophoretic parameters. It should be mentioned that the thermophoretic parameter Nt characterized as the physical meaning for the ambient temperature ratio to the characteristic wall temperature for a constant free stream velocity. The gradually

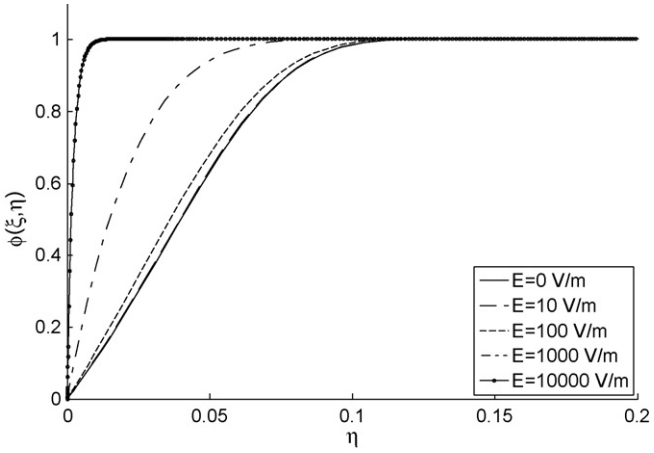

Fig. 3. Particle concentration profiles for different electric field strengths at $\xi = 1.0$, $n = 1.0$, $d_p = 0.1$ μm, $Ri = 1.0$, $\gamma = 2.01$, $\varepsilon = 0.45$, $a = 10$, $\kappa = 0.5$, $n_e = 1$, Nt = 1000.

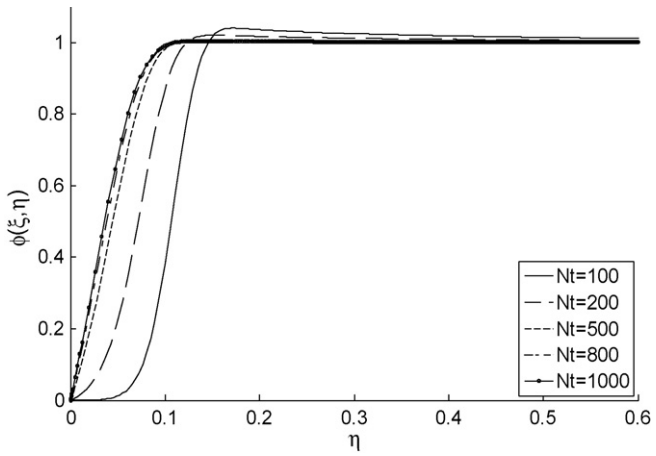

Fig. 4. Particle concentration profiles for different thermophoretic parameters at $\xi = 1.0$, $n = 1.0$, $d_p = 0.1$ μm, $Ri = 1.0$, $\gamma = 2.01$, $\varepsilon = 0.45$, $a = 10$, $\kappa = 0.5$, $n_e = 1$, $E = 100$ V/m.

increasing Nt is accompanied with a smaller thermophoretic effect and thinner concentration boundary layer thickness. In Fig. 4, it is seen that a zone free of particles is extended to about $\eta = 0.05$ at Nt = 100 and the profile may overshoot for particle size $d_p = 0.1$ μm. For the stronger electric field strength $E = 1000$ V/m in Fig. 5, the particle free layer is not seen in the profiles because of the enhancement suction effect due to electrophoresis.

Figs. 6 and 7 present the concentration profiles under the same electric field for various elementary charge numbers. The increasing n_e symbolizes the unit particle is charged with more electrons and thus apparently influenced by the electric field. This is why the increasing n_e coincides with the thinner boundary layer thickness and larger particle flux due to the electrostatic force direction.

Figs. 8 and 9 examine the combined effects on the concentration profiles to predict the particle sizes results from 0.01 to 1.0 μm. The larger particle size coincides with the larger particle Schmidt number and weaker particle diffusivity. The random mobility of large particle is small and leads to the thinner boundary layer thickness. The thinner boundary layer thickness also occurs more obviously due to the electric field strength enhancement, as shown in Fig. 9. While the particle diameter is about to 1.0 μm, the thermophoretic effect dominates the particle concentration at $\eta \to 0$, whereas for particle size smaller than 1.0 μm, electrophoresis plays a significant role.

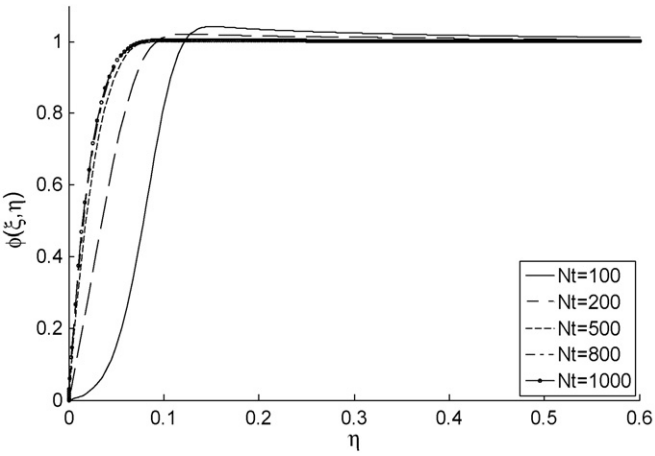

Fig. 5. Particle concentration profiles for different thermophoretic parameters at $\xi = 1.0$, $n = 1.0$, $d_p = 0.1$ μm, $Ri = 1.0$, $\gamma = 2.01$, $\varepsilon = 0.45$, $a = 10$, $\kappa = 0.5$, $n_e = 1$, $E = 1000$ V/m.

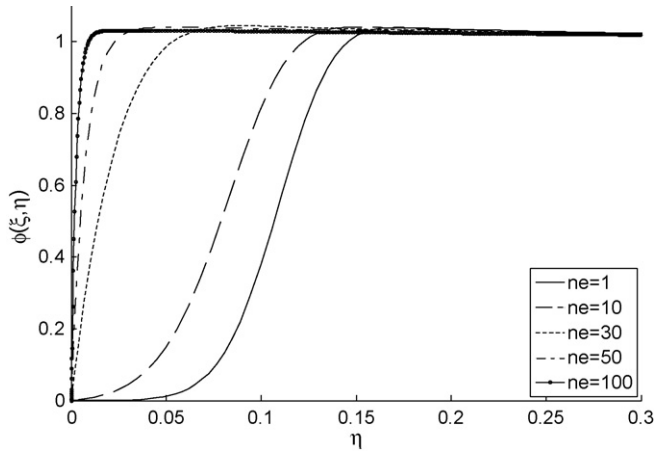

Fig. 6. Particle concentration profiles for different elementary charge numbers at $\xi = 1.0$, $n = 1.0$, $d_p = 0.1\ \mu m$, $Ri = 1.0$, $\gamma = 2.01$, $\varepsilon = 0.45$, $a = 10$, $\kappa = 0.5$, $E = 100\ V/m$, Nt = 100.

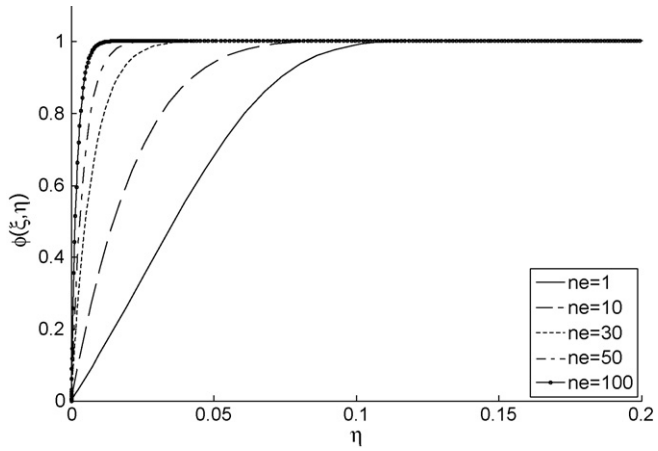

Fig. 7. Particle concentration profiles for different elementary charge numbers at $\xi = 1.0$, $n = 1.0$, $d_p = 0.1\ \mu m$, $Ri = 1.0$, $\gamma = 2.01$, $\varepsilon = 0.45$, $a = 10$, $\kappa = 0.5$, $E = 100\ V/m$, Nt = 1000.

Figs. 10 and 11 display the concentration profiles at Nt = 1000. From the curves it could be realized that the particle concentration is controlled by electric field and also influenced by the thermophoretic effect especially for particle size $d_p = 1.0\ \mu m$. This phenomenon is due to the blowing effect due to the temperature gradient. To make a comprehensive survey of Figs. 12–14, deposition velocities comparison onto a hot wall surface for particles sizes of $d_p = 0.01$–$1.0\ \mu m$ under various electric field strengths, thermophoresis and elementary charge numbers are illustrated. From the profiles, we can determine that the electrophoresis influence is huge for the selected particles. The increasing electric field

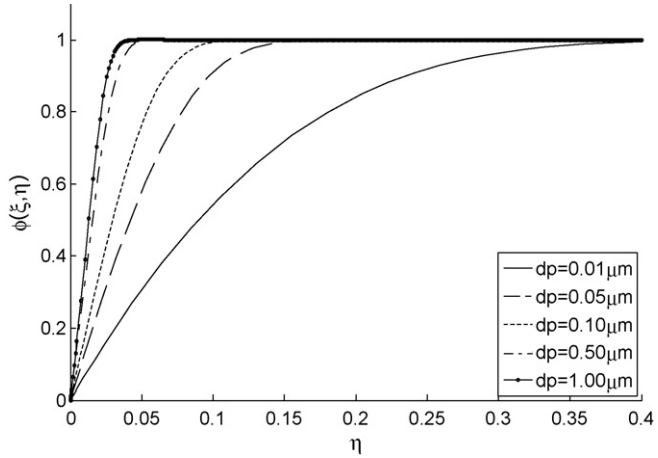

Fig. 8. Particle concentration profiles for different particle diameters at $\xi = 1.0$, $n = 1.0$, $Ri = 1.0$, $\gamma = 2.01$, $\varepsilon = 0.45$, $a = 10$, $\kappa = 0.5$, $n_e = 1$, $E = 100\ V/m$, Nt = 10000.

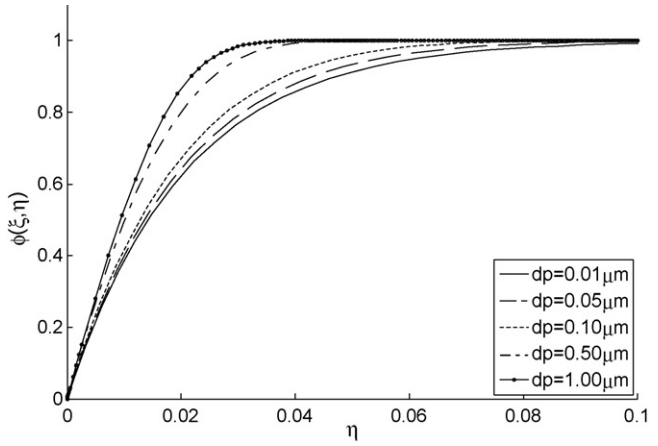

Fig. 9. Particle concentration profiles for different particle diameters at $\xi = 1.0$, $n = 1.0$, $Ri = 1.0$, $\gamma = 2.01$, $\varepsilon = 0.45$, $a = 10$, $\kappa = 0.5$, $n_e = 1$, $E = 1000\ V/m$, Nt = 10000.

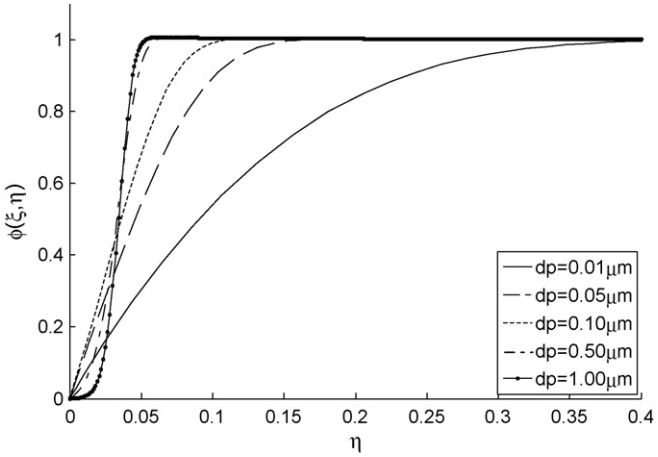

Fig. 10. Particle concentration profiles for different particle diameters at $\xi = 1.0$, $n = 1.0$, $Ri = 1.0$, $\gamma = 2.01$, $\varepsilon = 0.45$, $a = 10$, $\kappa = 0.5$, $n_e = 1$, $E = 100\ V/m$, Nt = 1000.

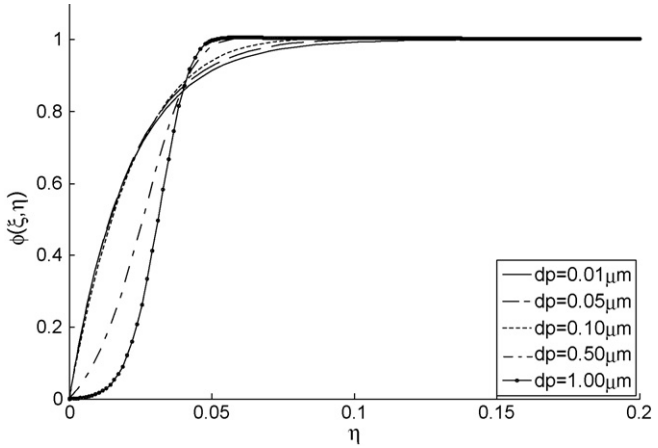

Fig. 11. Particle concentration profiles for different particle diameters at $\xi = 1.0$, $n = 1.0$, $Ri = 1.0$, $\gamma = 2.01$, $\varepsilon = 0.45$, $a = 10$, $\kappa = 0.5$, $n_e = 1$, $E = 1000\ V/m$, Nt = 1000.

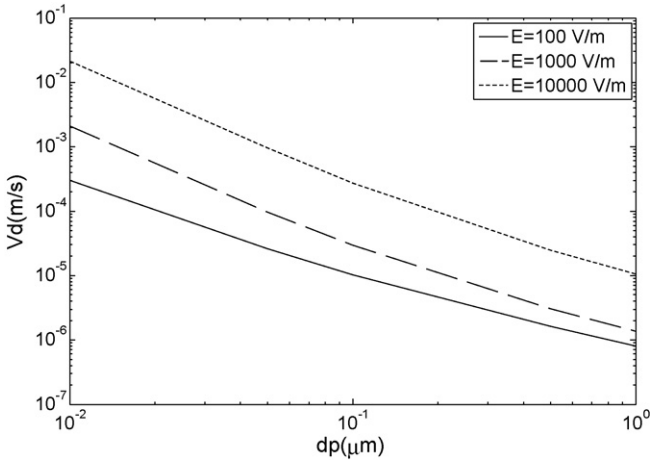

Fig. 12. Particle deposition velocity for different electric field strengths at $\xi = 1.0$, $n = 1.0$, $d_p = 0.01–1.00\ \mu m$, $Ri = 1.0$, $\gamma = 2.01$, $\varepsilon = 0.45$, $a = 10$, $\kappa = 0.5$, $n_e = 1$, Nt = 10000.

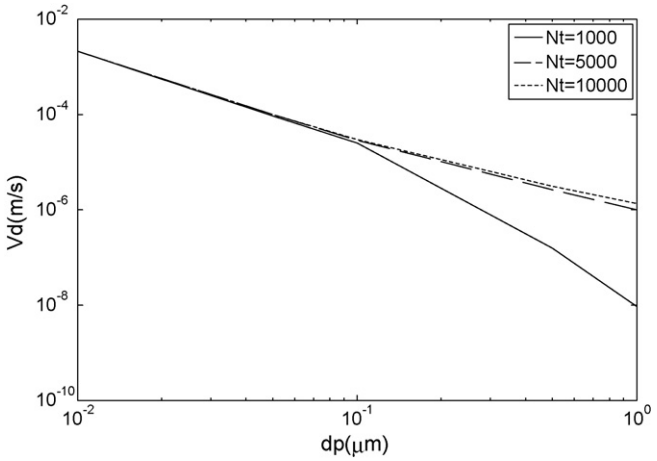

Fig. 13. Particle deposition velocity for different thermophoretic parameters at $\xi = 1.0$, $n = 1.0$, $d_p = 0.01–1.00\ \mu m$, $Ri = 1.0$, $\gamma = 2.01$, $\varepsilon = 0.45$, $a = 10$, $\kappa = 0.5$, $n_e = 1$, $E = 1000$ V/m.

strength and electron charge are accompanied with a larger particle deposition velocity. The thermophoretic force only dominates the mechanism for particle sizes of 0.1–1.0 μm. As Nt = 1000, the blowing effect is obviously seen for $d_p = 0.1–1.0\ \mu m$ because of the

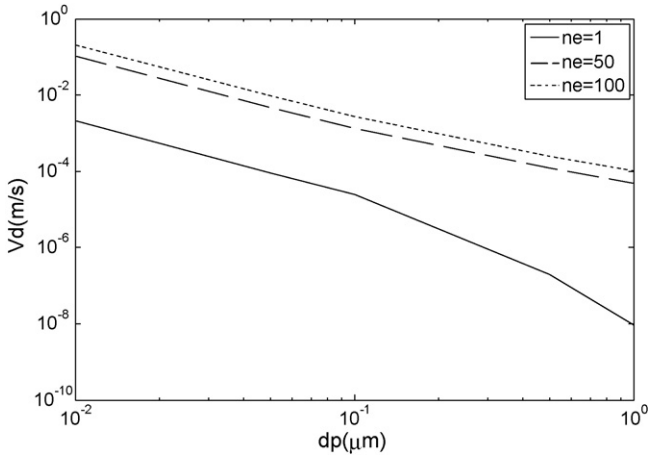

Fig. 14. Particle deposition velocity for different elementary charge numbers at $\xi = 1.0$, $n = 1.0$, $d_p = 0.01–1.00\ \mu m$, $Ri = 1.0$, $\gamma = 2.01$, $\varepsilon = 0.45$, $a = 10$, $\kappa = 0.5$, $E = 1000$ V/m, Nt = 1000.

Table 2
$\phi'(1,0)$ for various electric field strengths E at $n = 1.0$, $d_p = 0.1\ \mu m$, $Ri = 1.0$, $\gamma = 2.01$, $\varepsilon = 0.45$, a=10, $\kappa = 0.5$, $n_e = 1$, Nt = 100.

E (V/m)	0	10	100	1000	10000
$\phi'(1,0)$	0.0053	0.0056	0.0091	0.583	397

Table 3
$\phi'(1,0)$ for various thermophoretic parameters Nt at $n = 1.0$, $d_p = 0.1\ \mu m$, $Ri = 1.0$, $\gamma = 2.01$, $\varepsilon = 0.45$, $a = 10$, $\kappa = 0.5$, $n_e = 1$, $E = 100$ V/m.

Nt	100	200	500	800	1000
$\phi'(1,0)$	0.0091	1.19	8.07	11.5	12.8

Table 4
$\phi'(1,0)$ for various elementary charge numbers n_e at $n = 1.0$, $d_p = 0.1\ \mu m$, $Ri = 1.0$, $\gamma = 2.01$, $\varepsilon = 0.45$, $a = 10$, $\kappa = 0.5$, $E = 100$ V/m, Nt = 100.

n_e	1	10	30	50	100
$\phi'(1,0)$	0.0091	0.582	46.7	144	396

Table 5
$\phi'(1,0)$ for various particle diameters d_p at $n = 1.0$, $Ri = 1.0$, $\gamma = 2.01$, $\varepsilon = 0.45$, $a = 10$, $\kappa = 0.5$, $n_e = 1$, $E = 100$ V/m, Nt = 1000.

d_p (μm)	0.01	0.05	0.10	0.50	1.00
$\phi'(1,0$	6.84	11.6	12.8	2.31	0.10

driving away force from hot wall surface. The gradually increasing particle size responds to smaller deposition velocity due to the weaker mobility. Table 2 to 5 show the important results of $\phi'(1,0)$ for different electric field strengths magnitudes, thermophoresis, elementary charge numbers and particle sizes for each set of parameters. From the Tables 2 and 4, we can figure that as the increase of larger electric field strength and elementary charge number will lead to the steep concentration gradient due to the enhancement of the electrostatic driving force from the ambient to the wall. Table 3 depicts that the smaller Nt coincides with the stronger thermophoretic force away the surface under the constant electrostatic force as shown in Fig. 4. The particle diameters of 0.5 and 1.0 μm are significantly affected by the thermophoretic force than the other size listed in Table 5. The physical phenomenon also can be realized from the graphical profiles in Fig. 10.

4. Conclusions

We discussed the thermophoretic and electrophoretic effects on particle transport characteristics over a vertical flat wall from convective air flow through a porous medium. A theoretical model to describe the mass transfer phenomena for the combined transport mechanisms for diffusion, convection and the multiple effects mentioned above were investigated. The governing equations of momentum, energy and concentration are transformed using the appropriate similarity technique and numerical method. Interactive effects have been observed and described between the concentration profile and particle deposition velocity results. In summary, thermophoresis drives the particles away from the hot wall surface and the increasing electric field strength or electron charge lead to a larger electrophoretic velocity and thinner boundary layer thickness. This work provides a better analysis to understand the effects of thermophoresis and electrophoresis on particle deposition phenomena along a vertical flat wall through a porous medium. This is helpful for controlling aerosol particle technology and indoor air quality.

Acknowledgements

The authors are grateful to the National Science Council, Taiwan, for support through grant No. NSC 96-2221-E-033-038

References

[1] A.F. Mills, Heat and Mass Transfer, Irwin, New York, 1995.
[2] P. Goldsmith, F.G. May, Diffusiophoresis and thermophoresis in water vapour systems, in: C.N. Davies (Ed.), Aerosol Science, Academic Press, London, 1966, pp. 163–194.
[3] S.L. Goren, Thermophoresis of aerosol particles in the laminar boundary layer on a flat surface, J. Colloid Interface Sci. 61 (1977) 77–85.
[4] L. Talbot, R.K. Chenge, A.W. Schefer, D.R. Wills, Thermophoresis of particle in a heated boundary layer, J. Fluid Mech. 101 (1980) 737–758.
[5] A.J. Chamkha, I. Pop, Effect of thermophoresis particle deposition in free convection boundary layer from a vertical flat plate embedded in a porous medium, Int. Commun. Heat Mass Transfer 31 (2004) 421–430.
[6] M.A. Seddeek, Influence of viscous dissipation and thermophoresis on Darcy–Forchheimer mixed convection in a fluid-saturated porous media, J. Colloid Interface Sci. 293 (2006) 137–142.
[7] T.W. Peterson, F. Stratmann, H. Fissan, Particle deposition on wafers: a comparison between two modeling approaches, J. Aerosol Sci. 20 (1989) 683–693.
[8] M.H. Peters, D.W. Cooper, The effects of electrostatic forces on the thermophoretic suppression of particle diffusional deposition onto hot surfaces, J. Colloid Interface Sci. 140 (1990) 48–56.
[9] S.K. Friedlander, J. de la Mora, S. Gokoglu, Diffusive leakage of small particles across the dust-free layer near a hot wall, J. Colloid Interface Sci. 125 (1988) 351–355.
[10] S. Opiolka, F. Schmidt, H. Fissan, Combined effects of electrophoresis and thermophoresis on particle deposition onto flat surfaces, J. Aerosol Sci. 25 (1994) 665–671.
[11] R. Tsai, Y.P. Chang, T.Y. Lin, Combined effects of thermophoresis and electrophoresis on particle deposition onto a wafer, J. Aerosol Sci. 29 (1998) 811–825.
[12] R. Tsai, A simple approach for evaluating the effect of wall suction and thermophoresis on aerosol particle deposition from a laminar flow over a flat plate, Int. Commun. Heat Mass Transfer 26 (2) (1999) 249–257.
[13] P. Forchheimer, Wasserbewegung durch Boden, Forschtlft Ver. D. Ing. 45 (1901) 1782–1788.
[14] K. Vafai, C.L. Tien, Boundary and inertia effects on flow and heat transfer in porous media, Int. J. Heat Mass Transfer 24 (1980) 195–203.
[15] O.A. Plumb, J.C. Huenefeld, Non-Darcy natural convection from heated surfaces in saturated porous media, Int. J. Heat Mass Transfer 24 (1981) 765–768.
[16] R. Vasantha, I. Pop, G. Nath, Non-Darcy natural convection over a slender vertical frustum of a cone in a saturated porous medium, Int. J. Heat Mass Transfer 29 (1986) 153–156.
[17] S. Ergun, Fluid flow through packed columns, Chem. Eng. Prog. 48 (1952) 89–94.
[18] E.M. Sparrow, R. Eichhorn, J.L. Gregg, Combined forced and free convection in boundary layer flows, Phys. Fluids 2 (1959) 319–328.
[19] J.R. Lloyd, E.M. Sparrow, Combined forced and free convection flow on vertical surfaces, Int. J. Heat Mass Transfer 13 (1970) 434–438.
[20] P.H. Oosthuizen, R. Hart, A numerical study of laminar combined convective flow over flat plates, J. Heat Transfer 95 (1973) 60–63.
[21] P. Ranganathan, R. Viskanta, Mixed convection over horizontal flat plate embedded in a non-Darcy medium with suction and injection, Numer. Heat Mass Transfer 7 (1984) 305–317.
[22] J.Y. Jang, C.T. Shiang, The mixed convection plume along a vertical adiabatic surface embedded in a non-Darcian porous medium, Int. J. Heat Mass Transfer 40 (7) (1997) 1693–1699.
[23] E.M.A. Elbashbeshy, Laminar mixed convection over horizontal flat plate embedded in a non-Darcy medium with suction and injection, Appl. Math. Comput. 121 (2001) 123–128.
[24] E.M.A. Elbashbeshy, M.A.A. Bazid, The mixed convection along a vertical plate with variable surface heat flux embedded in porous medium, Appl. Math. Comput. 125 (2002) 317–324.
[25] E.M.A. Elbashbeshy, The mixed convection along a vertical plate embedded in non-Darcian porous medium with suction and injection, Appl. Math. Comput. 136 (2003) 139–149.
[26] Y.P. Chang, R. Tsai, F.M. Sui, The effect of thermophoresis on particle deposition from a mixed convection flow onto a vertical flat plate, J. Aerosol Sci. 30 (1999) 1363–1378.
[27] M.A. Selim, D.A. Hossain, S. Rees, The effect of surface mass transfer on mixed convection flow past a heated vertical flat permeable plate with thermophoresis, Int. J. Therm. Sci. 42 (2003) 973–982.
[28] H.C. Brinkman, A calculation of the viscous force exerted by a flowing fluid on a dense swarm of particles, Appl. Sci. Res. A1 (1947) 27–34.
[29] G.K. Batchelor, C. Shen, Thermophoretic deposition in gas flow over cold surfaces, J. Colloid Interface Sci. 107 (1985) 21–37.
[30] P.C. Reist, Aerosol Science Technology, 2nd ed., McGraw-Hill, New York, 1993.
[31] E. Isaacson, H.B. Keller, Analysis of Numerical Method, New York, 1966.
[32] T. Cebeci, P. Bradshaw, Physical, Computational Aspects of Convection Heat Transfer, Springer-Verlag, New York, 1984.